Limited reactivity of pyroxene and plagioclase in batch experiments with supercritical CO_2 in the presence of NaCl and $NaHCO_3$ in the context of CO_2 sequestration via carbonation

Zakhele H. Nkosi[a], Wladyslaw Altermann[b], Herbert Pölmann[c], Frédéric J. Doucet[d*]

[a] Department of Geology, University of Pretoria, Lynnwood Road, Pretoria 0002, South Africa

[b] Department of Geology, University of Johannesburg, P.O Box 524, Auckland Park 2006, South Africa

[c] Martin-Luther-University Halle-Wittenberg, Universitätsplatz 10, 06108 Halle (Saale), Germany.

[d] Council for Geoscience, Private Bag X112, Pretoria 0001, South Africa

[*] Correspondence author:

Frédéric J. Doucet, Tel.: +27 71 686 3932, Email: fdoucet@geoscience.org.za

Abstract

One-step high pressure and temperature direct aqueous mineral carbonation of tailings derived from mining of Platinum Group Metals in South Africa, requires a fundamental understanding of the reactivity of the most dominant mineral phases, i.e. pyroxene and plagioclase (66 wt.% and 12 wt% of the bulk rock respectively) that are typically found in these tailings. The silicate minerals pyroxene and plagioclase were sampled from a pyroxenite footwall mined with the ore-bearing UG2 and from Merensky Reefs outcropping in the eastern limb of the Bushveld Complex. These pyroxene and plagioclase grains were concentrated by gravity-separation from the orthopyroxenite bulk rock and batch-reacted in a sodium chloride (NaCl) brine saturated with pure carbon dioxide (CO_2) gas-only or seeded with sodium bicarbonate ($NaHCO_3$; as an additional CO_2 source) for 13 days at 100 ºC and 10 MPa. Pyroxene dissolved slightly but no weathering features were observed in plagioclase. Analyses of the filtrates obtained from the pyroxene sample in the absence of $NaHCO_3$ showed an increased concentration of magnesium and calcium ions in solution. However, they had also reached a cation saturation sealing. On the other hand, liquid samples from reactions where both CO_2 gas and $NaHCO_3$ were added to

the solution, exhibited a pronounced decrease in dissolved magnesium and calcium ions. XRD patterns of some of the post-reaction solids collected from the cation-depleted solution aliquots showed peaks of newly formed secondary magnesite and vermiculite. Moreover, the presence of magnesite was further confirmed by Raman shift analysis of the dried solid products. The formation of secondary magnesite was observed only in the experiments seeded with $NaHCO_3$, specifically where the pre-reaction solid was pyroxene rich. Some of the resultant fluid chemistry was corroborated by the geochemical model that simulated the reaction parameters using the Geochemist Work Bench (GWB) software. Overall, the results indicate low pyroxene dissolution, which leads to limited carbonation. These findings suggest that the carbonation of PGM tailings may be constrained under the evaluated physicochemical conditions.

Keywords:

CO_2 mineral sequestration, mineral carbonation, pyroxene, carbon dioxide, supercritical

1 Introduction

The concentration of carbon dioxide (CO_2) in the atmosphere has increased from *ca.* 278 ppm at the beginning of the industrial revolution to the current value of *ca.* 417.9 ppm (WMO 2023). In 2022, the total measured anthropogenic CO_2 emissions were approximately 40.7 Gt of CO_2 (Friedlingstein et al. 2024) up from the 2020 levels of around 37.4 Gt CO_2 emitted that year (Friedlingstein et al. 2023). The Intergovernmental Panel on Climate Change (IPCC 2018) assessed numerous mitigation scenarios from several integrated assessment models to model key Representative Concentration Pathways (RCPs) that chart the likely result in 80 years if the collective member states of the Paris Agreement pursue specific emission policies. The most ideal of these pathways (RCP 2.6) is attaining the desired climate-crises-averting global average temperature rise equal to or less than 2 ºC by 2100. If the world is to achieve such a bold and comparatively low global rise in average temperatures, the average annual CO_2 emissions must be eliminated from ~36 Gt to nil over the next 760 years (Fuss et al. 2014). Other interventions, such as the active removal of CO_2 from the atmosphere, may have to play an increasingly important role during this period (Fuss et al. 2014; Lomax et al. 2015; Galik 2020).

Mineral carbonation or CO_2 mineralisation, a type of greenhouse gas removal (GGR) technology, is one of several leading suite of such carbon dioxide removal (CDR) technologies (Lackner et al. 1995; Veetil and Hitch 2021; Kusin et al. 2022). The technology, when deployed, should mimic how nature has managed the flux of carbon in the atmosphere – through the weathering of mostly mafic silicate rocks and subsequent precipitation of carbonates on the Archean Earth's surface, naturally sequestering the CO_2, then at levels 1000's fold higher than today, (Altermann 2004, Altermann et al. 2011). Since the proposal of this idea by Seifritz (1990), a vast number of reviews and experiments have been devoted to *ex situ* mineral carbonation of natural rocks and mine tailings (e.g. Kelemen et al 2008; Olajire 2013; Naraharisetti et al. 2019; Gür 2022; Yadav and Mehra 2022), emphasizing the enormous role that mineral carbonation of rocks and especially mine waste materials can contribute to this process (e.g. Daval et al., 2011, Sissmann et al, 2014, Back et al., 2022, Bullock et al. 2022; Stockreef et al., 2022, Kularante et al., 2023, Power et al. 2024, and many more), which all describe similar experiments on various mafic rocks, mimicking the CO_2 burial processes during the Precambrian, when CO_2 levels in the atmosphere were so much higher than today.

The assessment of 'direct' aqueous ex-situ mineral carbonation (or direct aqueous carbonation – DAC) is at the core of this study, the focus being on the reaction of CO_2 with the target material and subsequent precipitation of carbonates, all in a one-step aqueous process like the one devised by O'Connor et al. (2005) and Gerdermann et al. (2007). The past research using this method (Munz et al. 2012; Gadikota et al. 2014; Sissmann et al. 2014; Gadikota et al. 2020), has evolved towards showing the key rate limiting (i.e., passivating layer) and rate promoting parameters (i.e., temperature, solution chemistry). However, several outsized limitations plague the scaling-up of this CDR procedure, with most prominent being the heterogeneity of the potential feedstock material (Bullock et al. 2022), negatively affecting the costs of reacting the materials with CO_2 to form the carbonate minerals in sufficient quantities to warrant piloting and commercialising (Power et al. 2014; Li et al. 2018). Vogeli et al. (2011) demonstrated the relative geochemical heterogeneity of tailings from various PGM mines within South Africa's vast platinum 'belt'. Characterisation of the mineral contents of these tailings, however, showed that the abundance of Mg-Ca-containing mafic minerals might have the potential for being used as CO_2 sinks and potentially making South Africa an essential and leading country in mineral carbonation technologies (Doucet et al. 2011, Bullock et al. 2023).

Several studies have experimented on minerals similar or comparable to those found in PGM tailings. O'Connor et al. (2001, 2004, 2005), Gerdemann et al. (2007), Gadikota et al. (2020)

tested several Mg, Ca, and Fe-bearing silicate minerals by subjecting them to direct aqueous carbonation under supercritical CO_2 conditions at varying reaction parameters. They found that target silicate minerals such as olivine, wollastonite, and serpentine had the highest reaction rates compared to other minerals tested. In addition, parameters such as the solution in which the reaction occurs, the pre-treatment process (milling or preheating), and the reaction temperatures and pressure are key rate-limiting/enhancing factors. Meyer et al. (2013) discovered that leaching of the target metals using several acids had little effect on the most abundant target mineral, orthopyroxene. Mohamed et al. (2016) obtained better results using a thermochemical method that used ammonium sulphate as chemical reagent to extract several major elements such as calcium and aluminium.

The role of mining waste materials as feedstock to mineral carbonation as a key player in CDR value chain is gaining much traction in the discourse of CDR (Power et al. 2024). South Africa is listed as one of the key future sites (Bullock et al. 2022, 2023) due to its longstanding history of mining, especially from the world's largest platinum-rich layered mafic intrusion (Zeh et al. 2015). However, there is a lack of research on the suite of minerals (such as magnesian-rich orthopyroxenes and calc-rich plagioclase) typically found in there. This study aims to add further understanding of how Mg- and Ca- rich minerals such as pyroxene and plagioclase respond to DAC experimental conditions, more specifically established net-carbonation promoting parameters namely, supercritical CO_2, saline and $NaHCO_3$ seeded experimental conditions. Can carbonates form when the feedstock minerals are exposed to the best DAC experimental parameters as outlined in previous studies? The results should spur on more comprehensive experimental work from other workers in South Africa and beyond.

2 Materials and methods

2.1. Material preparation and chemical reagents

Bulk rock samples of footwall and hanging wall pyroxenite from the Bushveld Complex, Rustenburg Layered Suite in the eastern limb, were retrieved from Booysendal mining operations (Fig. 1) located near Mashishing, South Africa. The pyroxenite rock samples were crushed using a jaw and roller crusher, which produced less than sand-grain-sized particles (< 2.0 mm) from the intergrown large, pegmatitic mineral mash (average crystal size > 5 mm). These particles were then density-separated using a heavy fluid (Bromoform – $CHBr_3$) with a specific gravity of 2.89 g cm^{-3} at room temperature. The average theoretical density of pyroxene minerals is about 3.43 g cm^{-3}, which is denser than that of feldspar minerals (2.63 g

cm^{-3}, Cairncross and McCarthy 2015); the separation resulted in the aluminosilicate grains (and other lighter minerals) floating to the surface of the heavy fluid and the inosilicates (and other heavier minerals) sinking to the bottom. The two fractions of the bulk rock sample (pyroxene concentrate and plagioclase concentrate) were separated (Fig. 2) and washed with acetone.

Table 1 Mineral composition of the whole rock and heavy mineral concentrates as determined by XRD. The mineral phases are listed and ranked according to their relative density.

Minerals	**Specific Gravity**[a]	**Percentage Composition (wt. %)**		
		Bulk Rock	**Pyroxene Concentrate**	**Plagioclase Concentrate**
Enstatite	3.43	66	74	4
Hornblende	3.41	3	5	n.d.
Augite	3.38	7	9	6
Biotite	3.00	5	n.d.	1
Talc	2.80	4	5	n.d.
Quartz	2.66	3	1	14
Plagioclase	2.63	12	6	76

[a] The specific gravities were obtained from Cairncross and McCarthy (2015); n.d. = not detected.

The semi-quantitative XRD analyses (Table 1) confirmed that the heavy fluid separation successfully increased the pyroxene phase by ~13.7 % and subsequently reduced the amount of cumulus plagioclase by over 50% compared to that of the bulk rock wt. %. Similarly, the plagioclase component was also optimised from ~ 12 wt. % in the bulk rock to ~76 wt. % in the concentrate. When conducting reruns of the XRD analyses on the pyroxene concentrate

samples, the pyroxene to plagioclase distribution varied around 94:6 wt. % ratio when normalised to 100%.

Reagent grade sodium chloride (NaCl), sodium bicarbonate ($NaHCO_3$), and acids were sourced from Thermo Fisher (Kandel) GmbH. Solid CO_2 was produced in the laboratory using a propriety machine that converted liquid CO_2 of 99.8% purity (supplied by Westfalen AG) into solid pellets of dry ice. Ultra-pure water with an electrical conductivity of < 1 µS cm^{-1} was used in all experiments.

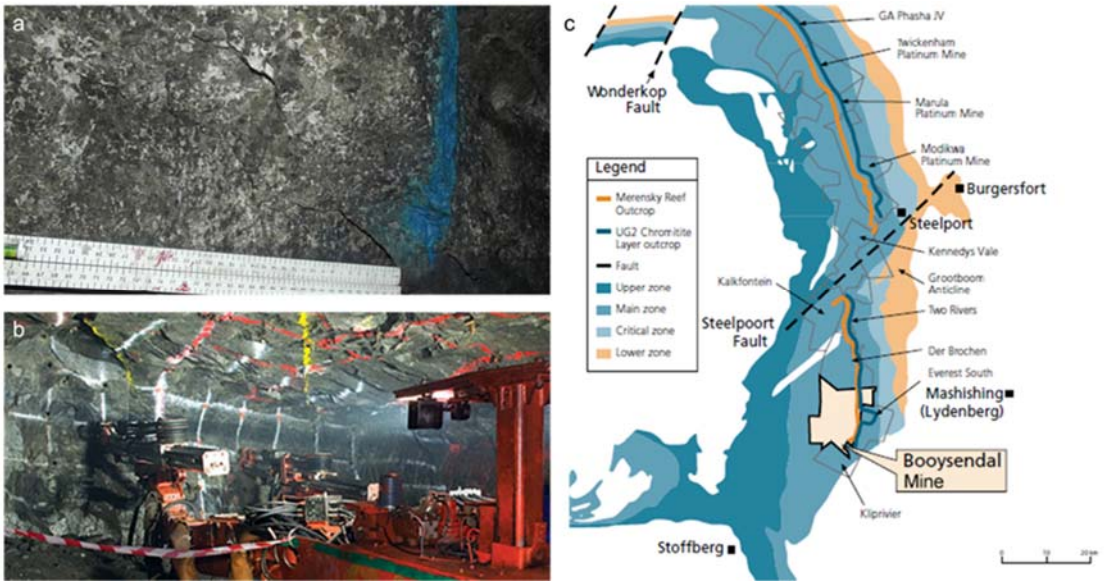

Fig. 1 Image of the (a) in-situ pyroxenite above the target ore, (b) samples collected during routine horizontal drilling exercise, and (c) geological map of the eastern limb showing the location of the Booysendal mine (Northam Platinum Holdings Limited 2023)

Fig. 2 Images of (a) pyroxenite whole rock hand specimen, which was crushed and underwent (b) heavy fluid separation, resulting in the two (c) lighter plagioclase and darker pyroxene concentrates.

2.2. Carbonation experiments

The static experiments were conducted in 36 cm^3 steel shell autoclaves (Berghof Products & Instruments GmbH) lined with Teflon (Fig. 3). The methodology was adapted from experimental designs employed in several previous studies that utilised low water-to-rock ratios (O'Connor et al. 2005; Gerdemann et al. 2007; Gadikota et al. 2014; Dawson et al. 2015; Tibane et al. 2021). Briefly, Experiment 1 consisted of immersing 2.0 g of milled dry samples of pyroxene or plagioclase concentrates in 10 mL ultrapure water (1:5 m/v solid-to-liquid ratio) containing 0.580 g NaCl(s). Experiment 2 was similar to Experiment 1, except that the NaCl solution also contained 0.538 g of $NaHCO_3$(s) seed which was added to allow the immediate availability of active CO_2 in the system. Before closing and sealing the autoclaves, CO_2 was charged in its solid state (dry ice). The equation of state (Equation 1; Peng and Robinson 1976), which is typically used to predict the vapour pressure and volumetric behaviour of pure or binary mixtures such as H_2O(l)-CO_2(sc), was applied to calculate the precise amounts of solid CO_2 needed to induce a partial pressure of 100 bar at 100 °C in the given headspace volume. The autoclaves were placed in an oven at 100 °C for 13 days.

$$\boldsymbol{p = \frac{R*T}{V_m - b} - \frac{a*\alpha}{V_m^2 - 2b*V_m - b^2}} \qquad \textbf{Equation 1}$$

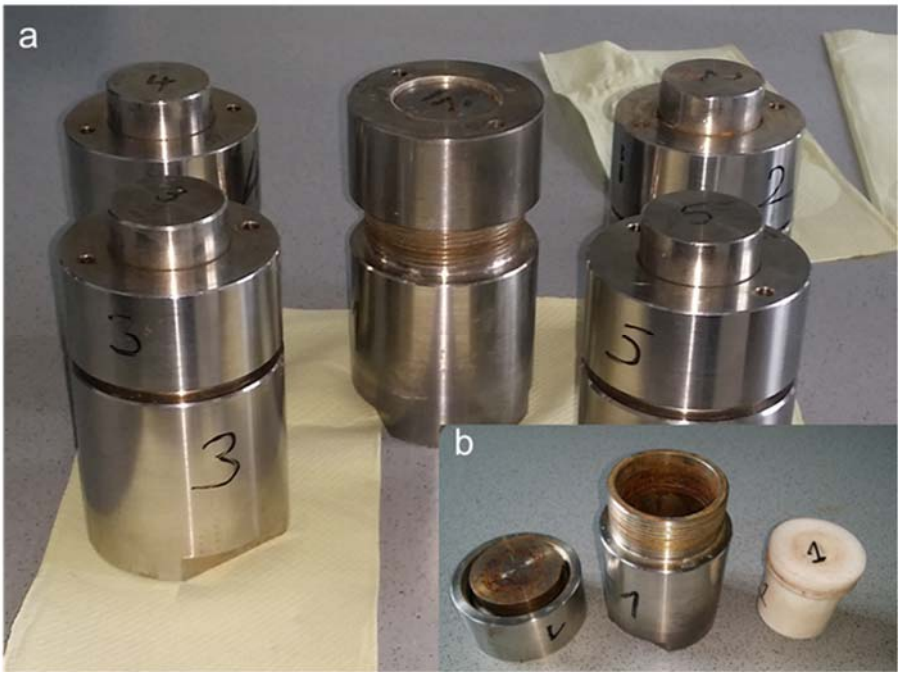

Fig. 3 Photographs of (a) high-temperature and pressure autoclaves, and (b) inner Teflon capsule used in experiments conducted at the Institute for Geosciences and Geography, Martin-Luther University, Halle-Wittenberg, Germany.

The experiments were conducted in a closed system where real-time reactions could not be observed or monitored. At the end of the 13 days, the autoclaves were removed from the oven and allowed to cool down to room temperature before further processing. The suspensions were filtered using Macherey-Nagel™ (MN 615) paper filter, which retained particles larger than *ca*. 8 µm. The filtrate was preserved at pH 1-2 by adding nitric acid (HNO_3). The solid residues were rinsed using ultrapure water until all the residual salts (NaCl and $NaHCO_3$) had been removed. Lead (II) nitrate was used to confirm the absence of residual salts at the end of the washing step. The rinsed residues were dried in a dry-air oven at 40 °C for three days.

In each experimental run (Fig. 4), the pyroxene concentrates were loaded in four autoclaves, and the plagioclase in the remaining autoclave as a control. Baseline measurements were conducted on both concentrate types, mixed with ultra-pure water and NaCl at room temperature and pressure. The resultant fluids and solids, and those derived from experiments 1 and 2, were also analysed.

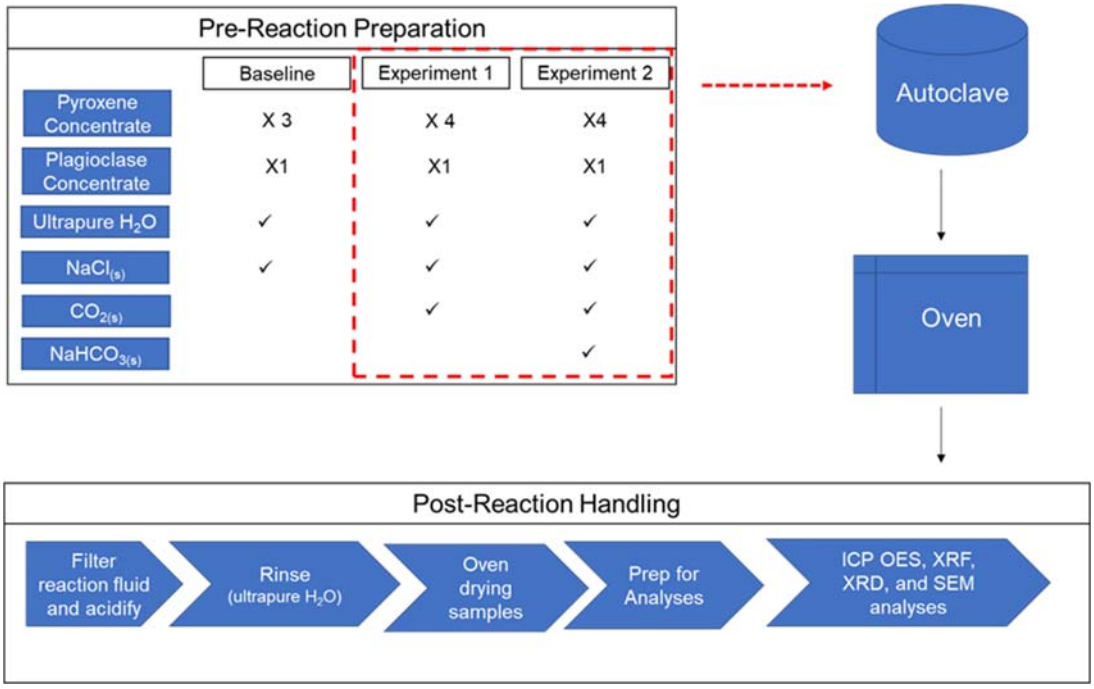

Fig. 4 A schematic flow chart of the experimental procedure

2.3. Analytical methods

2.3.1. Filtrates

The cation content (Ca, Mg, Fe, and K) of all filtrates from the baseline and autoclave experiments were analysed using the inductively coupled plasma optical emission spectrometer (ICP-OES) Plasma quant 110. The ICP-OES machine had a 3σ detection limit of 4.23 µg L^{-1}. Potassium was measured as a control cation, as it was anticipated to be the least mobile element in the system under high T/P conditions (Ho and Palmer 1987; Zimmerman et al. 2022).

2.3.2. Solid parent concentrates and residues

The heavy fluid-separated mineral concentrates were individually milled using a tungsten carbide milling pot and loaded at 50g per milling cycle. Each cycle was set at 1400 rpm for 60 seconds. The specific surface area of representative sub-samples was then analysed using the Brunauer, Emmet and Teller (BET) method with a Tristar II 3020™ Surface Area Analyser from Micromeritics™.

Elemental compositions were measured using an ARL Perfom'X Sequential X-ray fluorescence (XRF) spectrometer, and the Quantas™ software was used for data analysis. Before the

measurements, the samples were roasted at 1000 °C until they reached a constant mass. The difference between the initial and final mass was calculated to determine each sample's loss on ignition (LOI). One gram of each sample was carefully weighed and thoroughly mixed with 6 g of lithium borate ($Li_2B_4O_7$) flux in a platinum-gold crucible, then fused at 1050 °C to form a stable glass disk, which was subsequently analysed for its content in major and minor elements.

The mineral phases were measured using a Panalytical X'Pert^3 Powder with Pixcel 1D detector and Cu cathode. The XRD measurements were conducted with 45 kV and 40 mA, with fixed slits. The diffractograms were measured from 2 thetas 5º to 70º, with 18.87 s per step and a step size of 0.013º. The resultant diffractograms were processed using X'Pert Highscore Plus (v3.0.0) software. The peaks were manually evaluated and assigned since the software's automated peak detection algorithms were ineffective at discerning discrete peaks. The instrument has a limit of detection of ~ 0.01 wt %, thus crystalline phases present in amount below this value cannot be detected.

The Raman spectra measurements were done using a confocal Raman microscope (alpha300 R, WITec GmbH, Ulm, Germany) with a ~400 nm (lateral) resolution and an axial focus of ~ 1 μm. Photons produced by Rayleigh scattering and reflection were filtered out using a long-pass edge filter. A lens-based spectrometer measured the spectra with a CCD camera (1024 by 128 pixels), resulting in a resolution of 3.7 cm^{-1} per pixel from the detector using a 60 nm^{-1} grating. The laser excitation source was 2 mW (Nd: YAG laser), focused with a 20X objective (Nikon).

Scanning electron microscopy (SEM) analyses were performed using a JOEL JSM-6300 and a Bruker™ X-Flash EDX-detector (energy resolution of 125 eV) equipped with the Quantax 200 software. The Cameca SX100 electron probe microanalyser (EPMA), was used to obtain high resolution mineral chemistry, with settings: beam current between 38 and 40 nA, accelerating voltage of 20 kV, an electron beam size of 2 μm. Detection limits were ca. 0.2 mass% and monitored using the Cameca SX100 PeakSight software.

2.4. Geochemical modelling

The main objectives for modelling were to determine if a simplistic computer model would generate (dis)similar outcomes to what has been observed from the experimental results and to establish the likely kinetics operating during the closed-system reaction in which real-time reaction changes could not be observed. Additionally, the model was designed to predict dissolution kinetics based on the internal (e.g., Equation 2) rate laws. The proprietary

geochemical modelling software, Geochemist's Workbench (GWB™) version 2023, and more specifically the React® component, was used to model the geochemical (dissolution and precipitation) reaction processes that occurred between the mineral concentrates and the aqueous fluid medium. The default thermodynamic database, 'thermo.dat', was used, which employs the Dybe-Hückel equation calculating activity coefficients. Due to the introduction of salinity into the system (modelled and empirical), the 'salting-out' effect, which refers to the reduced solubility of a non-electrolyte/neutral species such as CO_2 should be accounted for in the GWB software, by way of introducing an activity coefficient of the neutral species (Allen et al. 2005). However, since the ionic strength of the model in this study was less than 3 mol/L (Allen et al. 2005), it is assumed that not accounting for this in our model, results in negligible internal CO_2 solubility estimates. In addition, the database contains equilibrium constants for the various reactions at the specific temperature and pressure conditions ranging from 0 – 300 °C and 1 – 100 bars, respectively (Bethke 1996).

The initial chemistry (Table 2) is outlined as close to its experimental analogue as reasonably possible and provides the basis of the initial fluid chemistry. Unlike the experiments, this reaction was simulated as occurring in a system containing 1 L of H_2O (instead of ~10 mL). Thus, the mineral-to-solution ratio was adjusted accordingly. To keep the model as simplistic as possible, in the pyroxene-rich computer model, for example, the kinetic enstatite was programmed as contributing 94 wt. % of the modal abundance and kinetic anorthite was described as the second most abundant mineral phase at 6 wt. % (vice versa). The other mineral phases were excluded from the model to limit the likely compounding error effect of using ideal kinetic data to represent the minerals (i.e., dissolution rates). The exclusion of said minerals (except for augite, which was treated as part of the total pyroxene phase) in the geochemical model meant that the total mass accounted for in the model was 175 g for both mineral concentrates according to the phase distribution displayed in Table 1.

Table 2 Initial input chemistry of the modelled batch reaction, with some variation between Experiment 1 and Experiment 2. For pre-experiment water quality, the Mg, Ca, and K cation concentrations were measured after the $NaHCO_3$ and NaCl were added to deionised water (possible impurities). The other parameters were calculated and estimated.

Chemistry	**Experiment 1**	**Experiment 2**
H_2O [Free kg]	1	1
$CO_{2(aq)}$ [molality]*	0.64	0.64
Ca^{2+} [$mg.kg^{-1}$]	0.01	0.01
Mg^{2+} [$mg.kg^{-1}$]	5.05	5.05
Cl^- [molality]**	1	1
Na^+ [molality]	1	1.64
K^+ [$mg.kg^{-1}$]	7.15	7.15
$SiO_{2(aq)}$ [$mg.kg^{-1}$]	0.01	0.01
Al^{3+} [$mg.kg^{-1}$]	0.01	0.01
HCO_3^- [molality]	0.01	0.64
pH	Swap $CO_{2(aq)}$ for H+	Swap $CO_{2(aq)}$ for H^+
Temperature [°C]	100	100

The high pressure was accounted for by setting CO_2 (aq) at the calculated amount derived from the solubility models by Duan et al. (2006). The systems' charge balance was not measured analytically; thus, it was balanced based on Cl^- ion activity. A fundamental rate law (Equation 2) was applied to calculate the dissolution and precipitation rate of the component kinetic phases in the model. The specific surface area of samples was measured to be 2.54×10^4 cm^2 g^{-1} (using the BET method), three measurement runs were conducted on a 2.8870 g sample after the concentrate samples were milled. The reaction rate constant is another physical parameter

that needed manual input; for enstatite, the pre-exponential factor (2.4 x 10^{-4} mol cm^{-2} s^{-1}) and activation energy (48.50 KJ mol^{-1}) were loaded instead of a direct rate constant value (Oelkers and Schott 2001), this allows the program to calculate a dynamic dissolution rate as the simulation progresses. On the other hand, only a fixed rate constant for plagioclase (specifically labradorite) could be determined from the literature (3.55 x 10^{-15} mol cm^{-2} s^{-1}; Black and Haese, 2012). This was the 'approach to equilibrium' or 'steady state' dissolution rate measured by the authors based on Si and Ca species derived from reacting a labradorite ($Na_{0.4}Ca_{0.7}Al_{1.5}Si_{2.5}O_8$) specimen in a saline solution at high temperature (80 ºC) and pressure (200 bar) (Black and Haese, 2012; 2014).

$$r_k = A_s k_+ \left(1 - \frac{Q}{K}\right) \qquad \textbf{Equation 2}$$

3 Results

3.1 Characterisation of starting materials

Based on the petrographic analyses (Fig. 5) and later confirmed by microprobe analyses, the plagioclase pyroxenite samples contained phaneritic crystals of orthopyroxene, clinopyroxene, plagioclase, quartz, and minor amounts of phlogopite, biotite, olivine, and opaque crystals (mostly chromite). The average orthopyroxene (Table 3) is highly magnesium-rich (Mg# ~80), typically dominated by enstatite endmember ($En_{77}Fs_{20}Wo_{03}$) chemistry. The calcium-rich pyroxene ($Wo_{47}En_{45}Fs_{08}$) plots on the augite region of the clinopyroxene nomenclature ternary system of Morimoto et al. (1988). The typical plagioclase is calcium-rich ($An_{67}Ab_{31}Or_{01}$), constraining most feldspar minerals in this study as labradorite in the continuous plagioclase series (Howie et al. 1992).

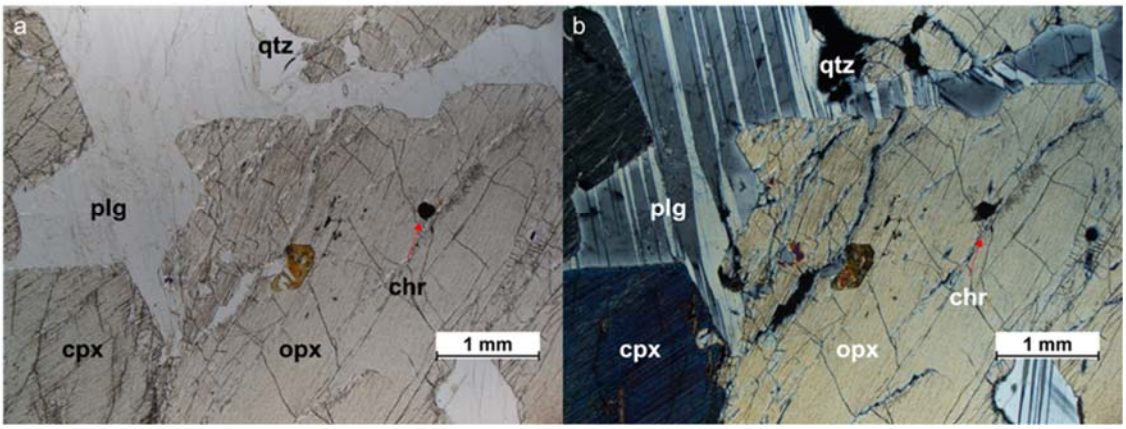

Fig. 5 Photomicrographs demonstrating the typical petrographic properties of pyroxenite's (a) anhedral chromite crystals in granular orthopyroxene with cumulus plagioclase and minor low-relief quartz in plane-polarised light; and (b) sizeable euhedral clinopyroxene in cross-polarised light

Table 3 Major element composition of eastern BIC footwall pyroxenite minerals

Oxides	**Bulk Rock[a] (n = 69)**	**Bulk Rock[b] (n = 2)**	**Orthopyroxene[c] (n = 19)**	**Clinopyroxene[c] (n = 22)**	**Plagioclase[c] (n = 19)**
SiO_2	54.80	51.45	55.14	52.30	51.20
TiO_2	0.20	0.20	0.16	0.33	0.04
Al_2O_3	1.03	5.37	1.44	2.70	30.26
Cr_2O_3	0.42	0.95	0.49	0.95	0.01
MgO	**29.20**	**24.50**	**28.48**	**15.68**	**0.03**
CaO	**1.41**	**3.91**	**1.44**	**22.78**	**13.96**
MnO	0.25	0.23	0.26	0.14	<0.01
FeO_t	**12.97**	**12.40**	**13.02**	**4.98**	**0.21**

NiO	0.10	0.12	0.11	0.06	0.01
Na_2O	0.02	0.41	0.02	0.36	3.58
K_2O	<0.01	0.19	<0.01	<0.01	0.26
Total	100.41	99.73	100.56	100.29	99.55

[a]*Values obtained from Mondal and Mathez (2007)*

[b]*Bulk rock oxide chemistry measured in this study using XRF*

[c]*Mineral oxide chemistry measured in this study using a microprobe*

3.2 Experimental water chemistry and elemental changes

3.2.1 Pyroxene concentrate

The baseline experiment using pyroxene concentrate provided reference observations for the chemical composition of filtrates when the concentrates had been suspended in a saline solution of NaCl at ambient temperature and atmospheric pressure for 13 days. A considerable variation in Mg concentration was observed between the filtrates generated by the triplicate baseline experiments, with values ranging between 77 – 170 mg. L^{-1} (Fig. 6a). In contrast, Ca varied over a narrower range (27 – 43 mg L^{-1}; Fig. 6b), and K varied tightly at ca. 224 mg L^{-1} (Fig. 6c). The iron cation was very low (< 1 mg. L^{-1}) in all baseline experiments.

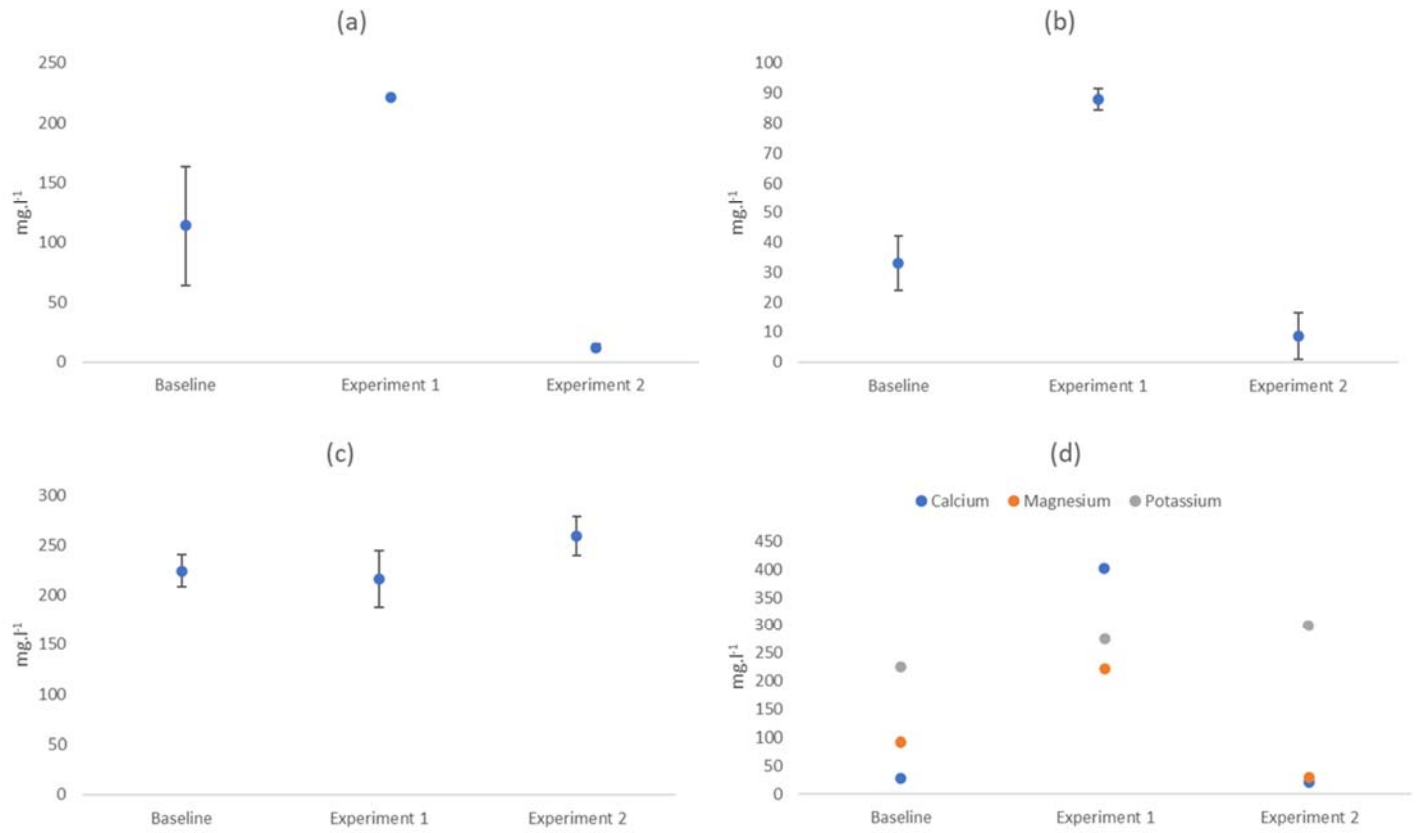

Fig. 6 Measured major aqueous ion mass concentrations (mg/L) where the concentration of (a) magnesium, (b) calcium, and (c) potassium are reported from all (quadruplicates) experiments where pyroxene concentrate powder was used. For the experiment-duplicate control, (d) plagioclase concentrate powder was also experimented upon without duplicate runs. The error bars on (a) – (c) are derived from standard deviation calculations of the quadruplicate results.

Exposing the mineral to higher temperature and pressure conditions of 100 °C and 100 bar in Experiment 1 resulted in an increased Mg concentration in the filtrate to ca. 222 mg L^{-1}, with the quadruplicates showing a very narrow error margin, as illustrated by the relatively tight error bar in Fig. 6a. In contrast, the filtrates generated during Experiment 2 with $NaHCO_3$ contained much less Mg (ca. 12 mg L^{-1}). Similar observations were made about Ca, with the filtrates from Experiments 1 and 2 containing elevated (ca. 88 mg L^{-1}) and low (ca. 9 mg L^{-1}) Ca concentrations, respectively (Fig. 6b). The content of K in all filtrates generated by the baseline and treatment experiments were broadly similar and was therefore unaffected by the changes in experimental conditions tested (Fig. 6c). The Fe ion in the filtrates was either very low (< 0.3 mg L^{-1}; Experiment 1) or undetected (Experiment 2).

3.2.2 Plagioclase concentrate

The baseline experiment using plagioclase concentrate was not duplicated due to the limited amount of material extracted from the host rock. The single experiment was, nevertheless, helpful in providing control observations, with the generated filtration containing 93 mg L^{-1} Mg, 28 mg L^{-1} Ca and 225 mg L^{-1} K, while Fe was not detected.

Figure 6d shows that the filtrates from Experiment 1 contained a higher Mg concentration (ca. 222 mg L^{-1}) compared to those from Experiment 2 (ca. 30 mg L^{-1}). Similarly, the Ca content was also found to have decreased substantially, from ca. 402 mg L^{-1} to ca. 21 mg L^{-1}. In contrast, the content of K in all filtrates generated by the baseline and treatment experiments had marginally increased.

3.3 Mineralogical changes

The morphology of the grains in the samples generated in Experiment 2 for the reacted plagioclase (Fig. 7b) and pyroxene concentrates (Fig. 7d) had a pronounced visual difference compared to those from the resultant samples generated in the baseline/unreacted counterparts (Fig. 7a and c). Various larger irregularly shaped grains were covered by a larger population of fine particles that had formed a thin coating layer at their surface. Using the SEM EDX probe, a semi-quantitative chemical spot analysis was conducted, from which 70 – 80 % of the chemistry of the newly formed finer particles belonged to that of the dominant mineral group

(pyroxene and plagioclase). Carbonate-like mineral phases were not observed, despite using a gold coating.

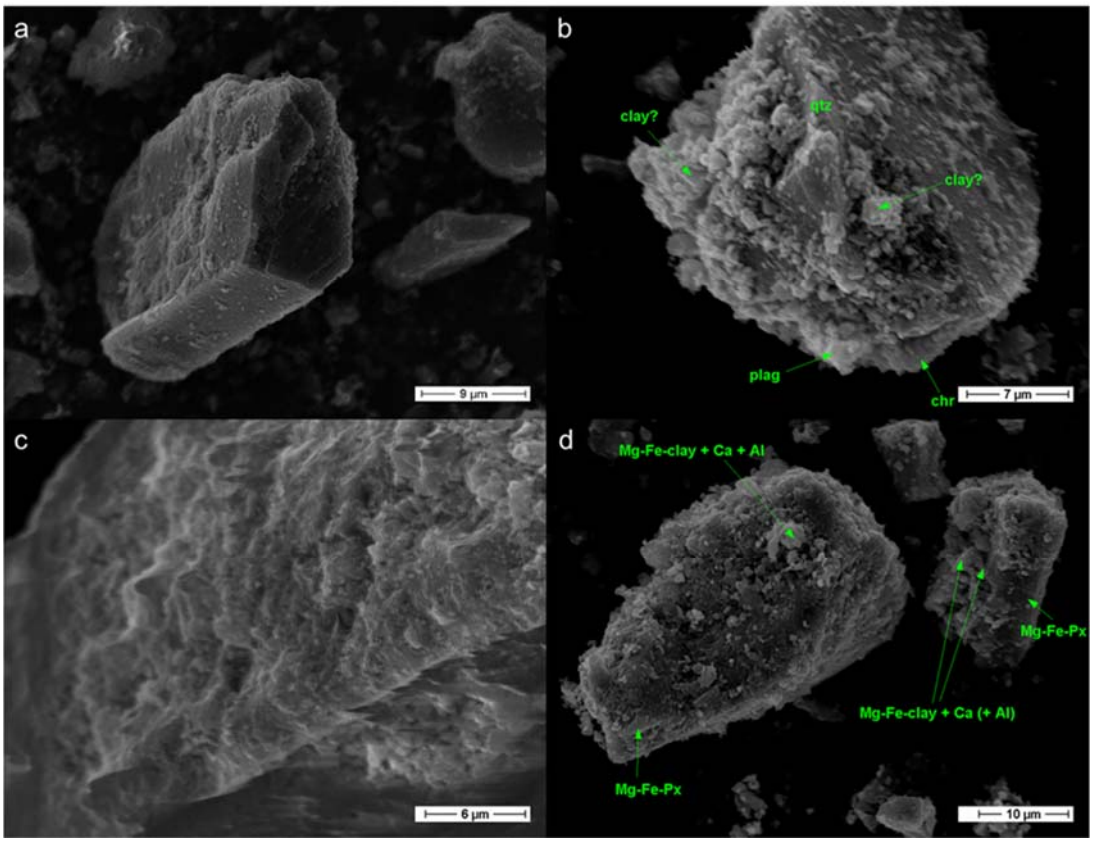

Fig. 7 Micrographs comparing the reacted and unreacted samples: (a) shows a typical unreacted plagioclase grain from the concentrate with 'residue-free' surfaces, and (b) is the reacted counterpart displaying grains with a surface covered by smaller crystallites (coating/residue); (c) demonstrates a unreacted pyroxene grain and (d) is another example of a post-reaction grain with a coating of various crystallites.

Table 4 A summary of the chemical alteration indices used in this study (modified from Price and Velbel, 2003)

Index	Formula	Optimum fresh value	Optimum altered value
CIA	$(100)(\frac{Al_2O_3}{Al_2O_3 + CaO + Na_2O + K_2O})$	≤ 50	100
CIW	$(100)(\frac{Al_2O_3}{Al_2O_3 + CaO + Na_2O})$	≤ 50	100
PIA	$(100)(\frac{Al_2O_3 - K_2O}{Al_2O_3 + CaO + Na_2O - K_2O})$	≤ 50	100

The residues from Experiments 1 and 2 for pyroxene concentrates were analysed by XRF to assess major-element chemical changes that may have occurred. Based on the bulk chemistry of the untreated and treated samples, the Chemical Index of Alteration (CIA), Chemical Index of Weathering (CIW), and Plagioclase Index of Alteration were used to gauge and compare the relative weathering effect of the experiments (Price and Velbel 2003). Each index (Table 4) incorporated various major element oxide chemistry into a unit-less integer ranging from 0 to 100 to show the relative degree of alteration. The alteration indices were calculated for untreated and treated samples. The untreated pyroxene concentrate indices are used as a reference point, with all three ranging from ca. 37 – 39 (Fig 8). On the other hand, the indices point towards a marginal increase in the extent of weathering/alteration of the samples of the treated pyroxene concentrate. The residues of Experiment 2 appear to be relatively more weathered than those from Experiment 1 and their corresponding untreated counterparts.

Fig. 8 Scatter plot showing several weathering indices for unreacted pyroxene concentrate, and the resultant samples after Experiments 1 and 2 for pyroxene concentrates (indices were adapted from Price and Velbel 2003).

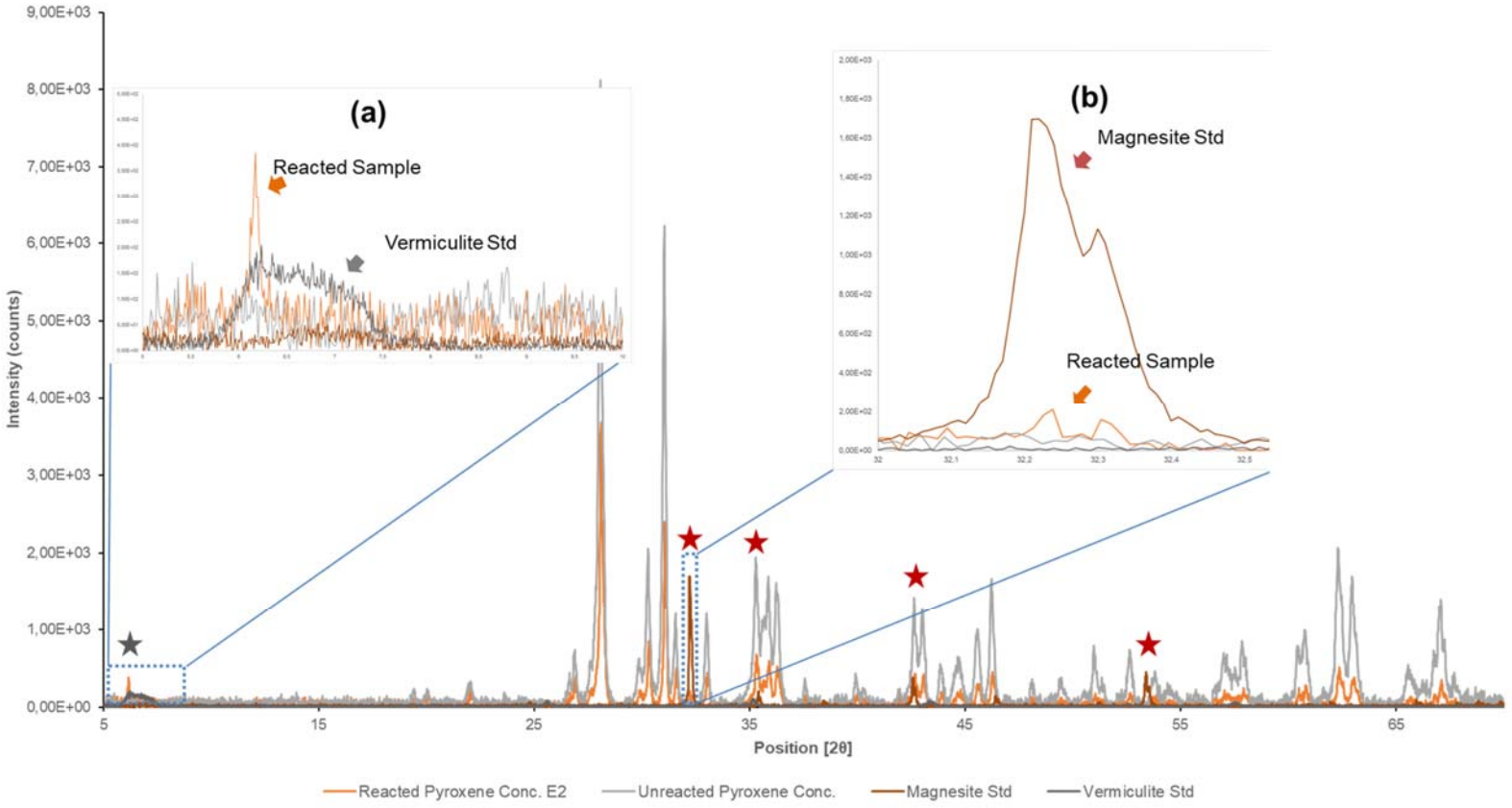

Fig. 9 XRD diffractograms for pyroxene-rich samples untreated and reacted (only post Experiment 2) and the two reference standards of vermiculite and magnesite. The magnified sections show the positions of secondary phases of (a) vermiculite and (b) magnesite in relation to the reacted pyroxene XRD pattern.

The XRD results showed that the reactions (especially those from Experiment 2 of the pyroxene concentrate) produced above detection limits of vermiculite and magnesite minerals. The XRD patterns of all treated samples were carefully assessed and compared to their untreated counterparts, and changes in peak shape and positions (indicative of new phases) were noted. The post-reaction samples of Experiment 1 displayed only the formation of vermiculite in three of the four post-reaction samples, but for Experiment 2 showed the presence of vermiculite in all the measured post-reaction pyroxene concentrates. Magnesite occurrence was identified in 3 out of 4 pyroxene experiment quadruplicates, but it (or any other carbonate) was not observed on the reacted plagioclase concentrate diffractogram. The XRD diffractograms of reacted pyroxene were overlaid with those of the two XRD standards (Lafuente et al. 2015) of vermiculite (R050490-1) and magnesite (R050443), which aligned perfectly with the identified phases (Fig. 9a and b).

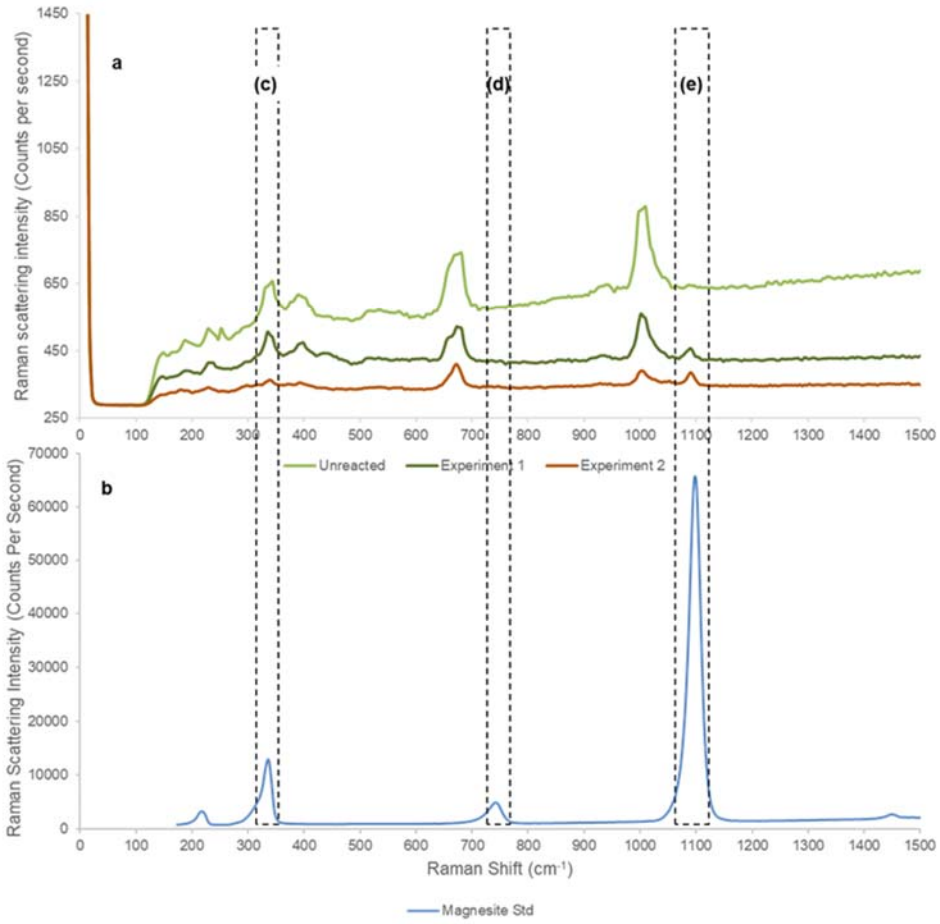

Fig 10 (a) Experimental Raman spectra of untreated and treated pyroxene concentrate, and (b) Spectral Raman reference pattern of magnesite (RRUFF ID: R040114).

Raman shift analysis was utilised to observe – through changes in the peak patterns, their positions, and relative intensities – any discrete phase changes and phase additions that some other techniques might have missed. Only the pre- and post-reaction samples of concentrated pyroxenes were analysed. The spectra from the reacted samples displayed relatively lower scattering intensities compared to the unreacted counterparts, with differences measured as much as ~500 counts/sec when comparing the highest peaks at around 1000 cm^{-1} wavelength position (Fig. 10a). The peak's position and shape, on the other hand, remained unchanged. However, a new peak was found at wavelength ~1100 cm^{-1} (Fig. 10e) from both the reacted samples of Experiments 1 and 2. The peak matched the frequency shift of CO_3^{2-} commonly observed between 1080 and 1100 cm^{-1} (Dufresne et al. 2018); the associated frequency shift between 120 and 450 cm^{-1} was not discernible. The reference pattern of magnesite provided the best possible match (Fig. 10b) compared to other carbonate reference standards. This was the only new phase that could be effectively identified using Raman spectroscopy.

3.4 GWB mineral reaction modelling

The interaction between the pyroxene concentrate suspended in brine and CO_2 in Experiments 1 and 2) was simulated as a simple model using the Geochemist Workbench software. The critical model outputs of interest were the changes in solution pH, dissolution and precipitation phases, and major element concentration over the 13 days (Fig. 11). The modelled Mg and Ca final concentrations are consistent with the data from both experiments in proportional and relative terms. A substantial dissolution of the model kinetic enstatite and anorthite is predicted to have occurred during Experiment 2, where $NaHCO_3$ was included. In addition, the highest precipitation of magnesite also took place in that second experiment model.

Since the pH was not measured during and after the experiments; the model allowed for the indirect observation of the pH kinetics in the batch reactors. According to the model, the pH in Experiment 1 was relatively more acidic for the whole duration of the experiment, rising and remaining above pH 4.9 after 0.001 days or 1.44 min (Fig. 11a), compared to the model of Experiment 2, which was buffered around pH 6 (Fig. 11b) for the entire duration of the model. Overall, both models suggest that the high CO_2 pressure conditions would result in an acidic reaction solution and only raise the pH by 1.3 orders of magnitude due to the presence of $NaHCO_3$. This is a similar output when simulating a plagioclase-rich scenario of both experiments (Fig. S2).

The geochemical model predicted that the conditions of Experiment 1 would result in substantially higher cation presence in the final aqueous solution (Fig. 11c and d) compared to Experiment 2, especially for Mg^{2+} (~ 398 mg L^{-1}), and relatively less so for Ca^{2+} (~ 38 mg L^{-1}). The model indicates that the increased dissolution kinetics of enstatite and precipitation of magnesite and dolomite (Fig. 11f) under the reaction parameters of Experiment 2 result in lower concentrations of Mg^{2+} (~ 3.6 mg L^{-1}) and Ca^{2+} (~ 0.5 mg L^{-1}). The above-baseline levels of concentration in cations in the model for Experiment 1, and their subsequent depletion in Experiment 2, mirror the results observed from their empirical counterparts (Fig. 6a and 6b).

The computer model produced similar predictions regarding changes in the final aqueous solution for the plagioclase-rich content. Specifically, the conditions in Experiment 1 resulted in a higher cation concentration in the final solution compared to the simulated conditions of Experiment 2. However, the results from the model without $NaHCO_3$ (Fig. S2c) indicate that the precipitation of dolomite (Fig. 3c) resulted in lower final Ca^{2+} concentration (53 mg L^{-1}) compared to Mg^{2+} concentration (392 mg L^{-1}). This finding somewhat contrasts with the empirical results (Fig. 6d), where the final measured solution showed a higher total dissolved calcium concentration (402 mg L^{-1}). Both the plagioclase-rich and enstatite-rich models for Experiment 1 predicted similar dissolved Mg levels in the final solution, aligning with the measured results.

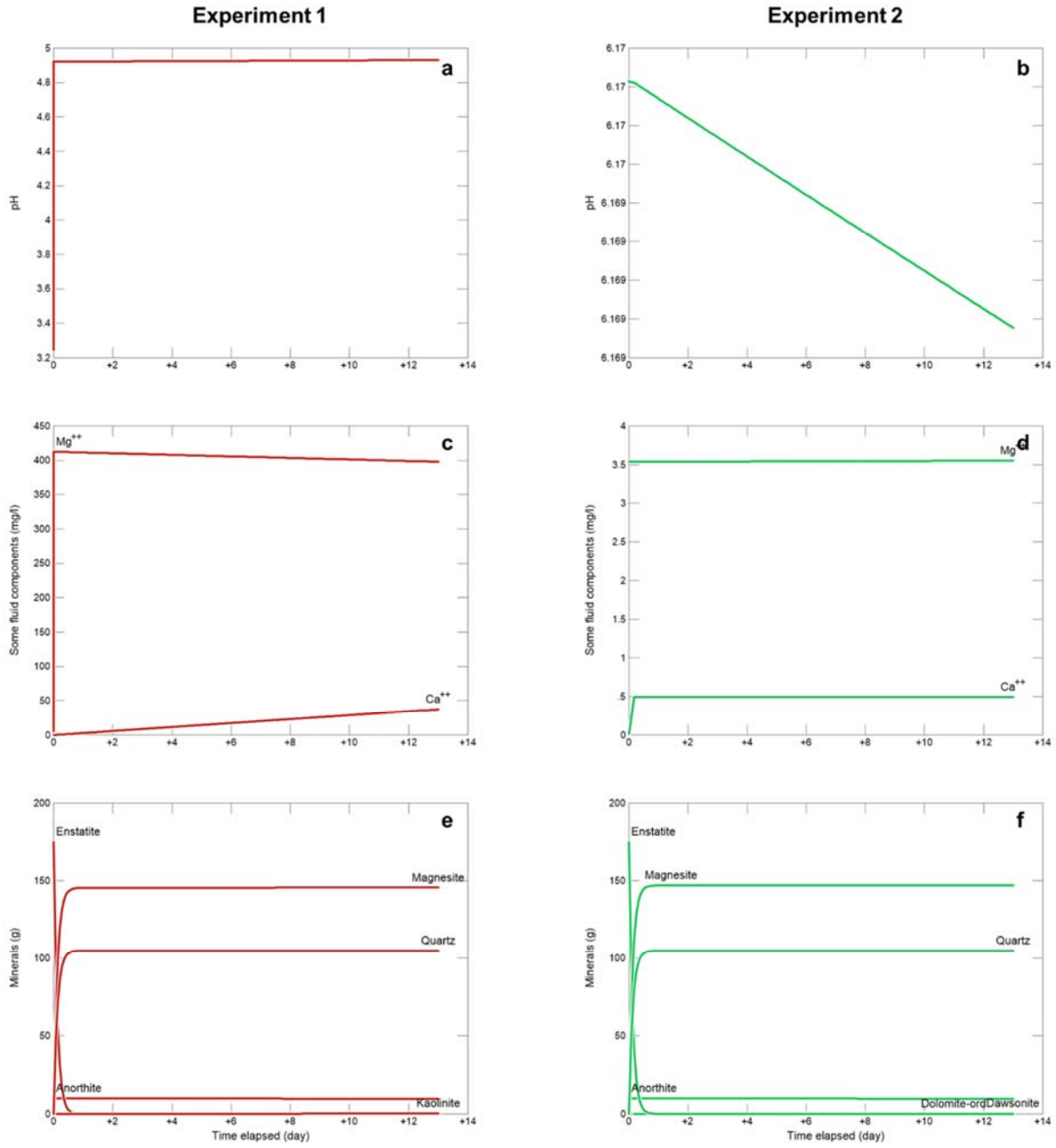

Fig. 11 The graphical outputs of the GWB model for the pyroxene reaction, with the simulated pH change of solution shown in a) and b). c) and d) indicate the evolution of Mg and Ca concentrations in the fluid over time; more specifically, the two graphs visualise the mass concentration limit in Experiment 1 and the cation depletion in Experiment 2 due to the presence of $NaHCO_3$. Graphs e) and f) show mineral phase changes (in mass) over time.

4 Discussion

The pyroxene concentrates displayed signs of weathering/dissolution as expressed by the alteration indices in Figure 8 when calculated using XRF data and the formulae (Table 4) outlined by Price and Velbel (2003). On the other hand, the plagioclase does not show such weathering pattern, as seen in Fig S1. However, the SEM observations on the residual sample did not reveal any evidence for dissolution, typically observed on surfaces of significantly digested minerals. The mineral surfaces, following the reaction, would typically show considerable corrosion, fracturing, or etch pit formation (Oelkers and Schott 1995; Monasterio-Guillot et al. 2021). Nevertheless, this does not preclude the possibility of dissolution, instead suggesting low dissolution rates or a different dissolution mechanism.

The observations from the batch reactions on pyroxene concentrate in Experiment 2, where $NaHCO_3$ was used, differed from those in Experiment 1 in that Mg and Ca mass concentrations were up to ~ 19 and ~10 times lower, respectively. On the other hand, when the same scenario was simulated using the GWB software, the model agreed with the observed experimental measurements; however, it computed the concentration of Mg and Ca 98 and 96 times lower, respectively. In addition, the computation predicted a preferential precipitation of magnesite and other carbonates (dawsonite and dolomite) with the increased concentration of dissolved CO_2. This was also analytically observed, where the magnesite phase was identified from the XRD and Raman spectra generated from the analyses of the solid residues from Experiment 2. The lower resultant cation concentration in Experiment 2 was correlated to conditions that favoured the precipitation of secondary carbonate minerals, thus depleting the cations from the aqueous solution, which confirmed the importance of the activity of $CO_{2(aq)}$ in promoting the precipitation of carbonates. In contrast, calcite (or other carbonate equivalents) was not precipitated (or above the detection limit of the instrument) in plagioclase-dominated control, where Ca^{2+} is the most active cation. Additionally, these results also support the findings of Gadikota et al. (2020) that suggest that the reactivity of Ca- and Na-bearing aluminosilicates is lower compared to Ca-, Mg- and Fe-bearing silicates. However, Munz et al. (2012) noted that there is a disaggregation between the dissolution of plagioclase and the precipitation of calcium carbonates, especially in batch reactions. The authors suggest that the limitation in precipitation of secondary calcium-carbonates may be rate-limited by the formation of proto-Al-hydroxides, gibbsite, and clays.

The cation activity and its effect on precipitation kinetics of carbonates were studied by several researchers (Giammar et al. 2005; Hanchen et al. 2008; Prigiobbe and Mazzotti 2013), who

observed that magnesite could directly precipitate at a relatively fast rates provided that the system is supersaturated with the carbonate mineral phase under high temperature and pressure conditions (90 – 120 °C, ~100 bar P_{CO_2}). For example, Giammar et al. (2005) measured the critical saturation index of magnesite to be 0.25 – 1.14 at 90 °C and 100 bar P_{CO_2} conditions. The research demonstrated that the loss of Mg cation from solution during carbonate precipitation is rate-limited by nucleation (and subsequent crystal growth of magnesite). Therefore, in this study, the Mg cation "mass concentration limit" of ca. 222 mg L^{-1} observed in Experiment 1 may be related to magnesite's precipitation-dissolution equilibrium barrier due to the limited supply of [CO_3^{-2}] in the system when compared to experiments that contained $NaHCO_3$.

The computer-generated model for Experiment 2 calculated a comparatively more alkaline-buffered pH for the solution when $NaHCO_3$ was added, suggesting that precipitation kinetics potentially occurred during the reaction. Compared to its low pH and analogue without $NaHCO_3$, the acidity potentially limits the possibility of carbonate precipitation. This may explain why Experiment 2 results in the near-total depletion of the mass concentration of the cations in solution and the emergence of a new mineral phase, magnesite.

The computational and experimental data suggest that the key factors that play a catalytic or inhibiting role in the kinetics of magnesite precipitation include pH and ionic strength of the bulk solution. In the case of pH, Giammar et al. (2005) demonstrated that the saturation index of magnesite was dependent on the pH; that is, the activity of [CO_3^{2-}] is tethered to that of [H^+], assuming a system that has reached equilibrium. Therefore, if the solution is less acidic, it is more favourable to magnesite nucleation and crystal growth. In addition, under saline conditions (increased ionic strength), magnesite formation is favoured due to the dehydration effect due to salinity, which readily allows the Mg^{2+} ion to pair with a [CO_3^{2-}] anion. The salinity decreases the double layer around the active complexes, thus facilitating the mobility of reactants to, and from the nucleating sites (Sayles and Fyfe 1973).

Unfortunately, due to the limited availability of sample material (no duplicates could be conducted) for the plagioclase-rich sample, certain analyses, such as XRD, could not be performed on the small subsamples. Consequently, this study cannot confirm whether the physical experiments would have resulted in the formation of new phases under these experimental conditions. However, the computer models provide valuable insights, suggesting that the conditions in Experiment 2 on the plagioclase-rich sample would likely favour the formation of more dolomite (ca. 18 times more) and dawsonite (ca. 17 times more) compared

to the pyroxene-rich model. This can be attributed to the greater availability of calcium and aluminium cations as they are released from the increased aluminosilicates reactive surface area (Oelkers and Schott 1995).

Both ortho- and clino- pyroxene minerals contained iron cations in their mineral structure. Therefore, the dissolution and subsequent release of Mg^{2+} to the solution should have resulted in a possible release of Fe. However, the dissolved Fe concentrations in most experiments were below the detection limit, which may suggest that the metal was precipitated out of the solution as iron oxide or there was a preferential incongruent release of Mg, relative to Fe. The former is supported by observations from experiments conducted by workers such as O'Connor et al. (2005) and Gadikota et al. (2014), who argue that the low solubility of iron oxide inhibits the formation of siderite in experiment setups similar to the one done in this study.

The GWB model predicted kaolinite and quartz as the likely none-carbonate mineral phases to form under Experiment 1 conditions. Quartz was the only non-carbonate mineral phase to form under Experiment 2 computational conditions, which affirms the net positive mineral carbonation effect of solutions buffered using sodium bicarbonate. However, this was not experimentally observed in this study, in that only the phyllosilicate, vermiculite, was formed (or was above the instrument's detection limit) in both experiments. This hydrous magnesium-aluminium-iron phyllosilicate likely formed from the alteration (vermiculitisation) of primary rock-forming minerals such as biotite (Wilson, 2004).

5 Conclusion and recommendations

The results from the experiments with $NaHCO_3$ as an additional source of carbonate anions point towards a system with preferential precipitation of magnesite, but possibly limited or no precipitation of Ca-bearing carbonates (i.e. dolomite or calcite). The higher mass concentration of magnesium is derived from the dissolving pyroxene minerals, thus resulting in the increased activity of Mg^{+2} ions, which are complexed with the well-supplied carbonate anions. In addition, the increased pH is likely to have been more favourable to magnesite nucleation and crystal growth. The plagioclase-rich sample (for Experiment 1 conditions) produced nearly double the dissolved cations in solution compared to pyroxene. This may suggest that either the calcium is less likely to form secondary minerals or that the plagioclase mineral has comparably higher dissolution rates relative to the pyroxene. Therefore, it is recommended that the dissolution rates of the samples and subsequent precipitation of carbonate minerals in CO_2-

H_2O/brine systems be investigated further to understand the kinetics that promote the forward mineral carbonation in the context of batch reaction experiments. However, this study showed that it is possible to produce stable carbonate minerals from DAC of pyroxene-rich materials, albeit the reaction kinetics are sensitive to the supply of CO_2 and the activity of the different cation species, and possibly other factors, such as the water-to-solid ratio.

Detection and identification of solid reaction products were challenging. In particular, the excited volume in the SEM-EDX analyses was likely to have included a substantial part of the original grains while the use of gold coating may have impacted the yield of light elements. In addition, the XRD evidence of the absence/presence of secondary minerals was not especially strong due to the inadequate availability of some post-reaction samples, especially for plagioclase concentrate experiments.

Overall, the results indicate low pyroxene dissolution, and consequently limited carbonation. These findings suggest that the carbonation of PGM tailings may be restricted under the evaluated physicochemical conditions.

Acknowledgements

This work is based on the research supported by CIMERA (DST-NRF Centre of Excellence for Integrated Mineral and Energy Resources Analysis) and the National Research Fund through the DAAD-NRF scholarship programme. The analytical work in this research would not be possible without the assistance of academics and technicians of the Martin-Luther Universität Halle (Department of Geosciences and Geography), Technische Universität Darmstadt (Physics of Surfaces Department), the University of Pretoria (Stoneman Analytical Lab) and the University of Johannesburg (SPECTRUM Lab). The authors thank the Council for Geoscience for providing supervisory assistance, insight, and expertise. Opinions expressed and conclusions arrived at are those of the author and are not necessarily to be attributed to the DAAD-NRF.

References

Allen DE, Strazisar BR, Soong, Y, Hedges SW (2005) Modeling carbon dioxide sequestration in saline aquifers: Significance of elevated pressures and salinities. Fuel Process Technol 86: 1569-1580. https://doi.org/10.1016/j.fuproc.2005.01.004

Altermann W (2004) Evolving life and its effect on Precambrian sedimentation. In: Eriksson PG, Altermann W, Nelson DR, Mueller W Catuneanu O (Eds.) Chapter 6.3: The Precambrian Earth: Tempos and Events. Developments in Precambrian Geology 12, Elsevier, 539-545.

Altermann W, Doucet FJ, Van der Merwe EM, Drobek T, Stark R, Tibane V (2011) The CO_2-rich Precambrian atmosphere and CO_2 sequestration in South Africa. 23rd Colloquium of African Geology (23rd CAG), Internat. Conf. Geol. Soc. Africa, University of Johannesburg, Abstracts Volume, p. 7.

Bethke CM (1996) Geochemical Reaction Modeling: Concepts and Applications. Oxford University Press, Oxford.

Back J, Zevenhoven R, Fagerlund J, Sorjonen-Ward P (2022). Mineral Carbonation Using Mine Tailings-a Strategic Overview of Potential and Opportunities. In Proceedings of the 16th Greenhouse Gas Control Technologies Conference (GHGT-16) (pp. 23-24).

Black JR, Haese RR (2012) Mineral dissolution experiments: GaMin'11 Interlab Round Results. Cooperative Research Centre for Greenhouse Gas Technologies, Canberra, Australia, CO2CRC Publication Number RPT12-3839, 41 pp.

Black JR, Haese RR (2014) Batch reactor experimental results for GaMin'11: Reactivity of siderite/ankerite, labradorite, illite and chlorite under CO_2 saturated conditions. Energy Procedia 63: 5443-5449. https://doi.org/10.1016/j.egypro.2014.11.575

Bullock LA, Yang A, Darton, R C (2022) Kinetics-informed global assessment of mine tailings for CO_2 removal. Sci Total Environ 808: 152111. https://doi.org/10.1016/j.scitotenv.2021.152111

Bullock LA, Nkosi Z, Vele M, Amponsah-Dacosta M (2023) Catalogue of South African mine tailings for geochemical carbon dioxide removal purposes. Int J Greenh Gas Control 124: 103844. https://doi.org/10.1016/j.ijggc.2023.103844

Cairncross B, McCarthy T (2015) Understanding Minerals & Crystals. Penguin Random House South Africa, Cape Town.

Daval D, Sissmann O, Menguy N, Saldi, G D. Guyot F, Martinez I, Hellmann, R (2011) Influence of amorphous silica layer formation on the dissolution rate of olivine at 90 C and elevated pCO_2. Chem Geol 284: 193-209

Dawson GKW, Pearce,JK, Biddle D, Golding SD (2015) Experimental mineral dissolution in Berea Sandstone reacted with CO_2 or SO_2–CO_2 in NaCl brine under CO_2 sequestration conditions. Chem Geol 399: 87-97. https://doi.org/10.1016/j.chemgeo.2014.10.005

Doucet FJ (2011) Scoping Study on CO_2 Mineralization Technologies. Report number CGS-2011-007, Council for Geoscience, Pretoria

Duan Z, Sun R, Zhu C, Chou IM (2006) An improved model for the calculation of CO_2 solubility in aqueous solutions containing Na^+, K^+, Ca^{2+}, M^{g2+}, Cl^-, and SO_4^{2-}. Mar Chem 98: 131-139. https://doi.org/10.1016/j.marchem.2005.09.001

Dufresne WJ, Rufledt CJ, Marshall CP (2018) Raman spectroscopy of the eight natural carbonate minerals of calcite structure. J Raman Spectrosc 49: 1999-2007. https://doi.org/10.1002/jrs.5481

Friedlingstein P, Jones MW, O'Sullivan M et al (2022) Global Carbon Budget 2021. Earth Syst Sci Data 14: 1917-2005. https://doi.org/10.5194/essd-14-1917-2022

Friedlingstein P, O'Sullivan M, Jones MW et al (2023) Global Carbon Budget 2023. Earth Syst Sci Data 14: 5301-5369. https://doi.org/10.5194/essd-15-5301-2023

Fuss S, Canadell JG, Peters GP, Tavoni M, Andrew RM, Ciais P, Jackson RB, Jones CD, Kraxner F, Nakicenovic N, Le Quéré C, Raupach MR, Sharifi A, Smith P, Yamagata Y (2014) Betting on negative emissions. Nat Clim Change 4: 850-853. https://doi.org/10.1038/nclimate2392

Gadikota, G, Matter, J, Kelemen, P, Brady, P V, Park, A H A (2020) Elucidating the differences in the carbon mineralization behaviors of calcium and magnesium bearing alumino-silicates and magnesium silicates for CO_2 storage. Fuel 277: 117900. https://doi.org/10.1016/j.fuel.2020.117900

Gadikota G, Matter J, Kelemen P, Park AH (2014) Chemical and morphological changes during olivine carbonation for CO_2 storage in the presence of NaCl and $NaHCO_3$. Phys Chem Chem Phys 16: 4679-93. https://doi.org/10.1039/C3CP54903H

Galik CS (2020) A continuing need to revisit BECCS and its potential. Nat Clim Change 10: 2-3. https://doi.org/10.1038/s41558-019-0650-2

Gerdemann SJ, O' Connor WK, Dahlin DC, Penner LR, Rush H (2007) Ex situ aqueous mineral carbonation. Environ. Sci. Technol. 41: 2587-2593. https://doi.org/10.1021/es0619253

Giammar DE, Bruant Jr RG, Peters CA (2005) Forsterite dissolution and magnesite precipitation at conditions relevant for deep saline aquifer storage and sequestration of carbon dioxide. Chem Geol 217: 257-276. https://doi.org/10.1016/j.chemgeo.2004.12.013

Gür TM (2022) Carbon dioxide emissions, capture, storage and utilisation: Review of materials, processes and technologies. PECS 89: 100965. https://doi.org/10.1016/j.pecs.2021.100965

Hänchen M, Prigiobbe V, Baciocchi R, Mazzotti M (2008) Precipitation in the Mg-carbonate system - effects of temperature and CO_2 pressure. Chem Eng Sci 63: 1012-1028. https://doi.org/10.1016/j.ces.2007.09.052

Ho PC, Palmer DA (1997) Ion association of dilute aqueous potassium chloride and potassium hydroxide solutions to 600°C and 300 MPa determined by electrical conductance measurements. Geochim. Cosmochim. Acta 61: 3027-3040. https://doi.org/10.1016/S0016-7037(97)00146-4

Howie R, Zussman J, Deer W (1992) An introduction to the rock-forming minerals. Longman London, UK.

IPCC (2018) Global Warming of 1.5°C. An IPCC Special Report on the impacts of global warming of 1.5°C above pre-industrial levels and related global greenhouse gas emission pathways, in the context of strengthening the global response to the threat of climate change, sustainable development, and efforts to eradicate poverty, Intergovernmental Panel on Climate Change.

Kelemen P B, Matter J. (2008) In situ carbonation of peridotite for CO_2 storage. Proc Natl Acad Sci USA 105: 17295-17300.

Kularatne K, Sissmann O, Guyot F, Martinez I (2023) Mineral carbonation of New Caledonian ultramafic mine slag: Effect of glass and secondary silicates on the carbonation yield. Chem Geol 618: 121282

Kusin FM, Hasan SNMS, Molahid VLM, Yusuff FMY, Jusop S (2022) Carbon dioxide sequestration of iron ore mining waste under low-reaction condition of a direct mineral carbonation process. Environ Sci Pollut Res 30, 22188–22210. https://doi.org/ 10.1007/s11356-022-23677-3

Lackner KS, Wendt CH, Butt DP, Joyce Jr EL, Sharp DH (1995) Carbon dioxide disposal in carbonate minerals. Energy 20: 1153-1170. https://doi.org/10.1016/0360-5442(95)00071-N

Lafuente B, Downs R., Yang H, Stone N (2015) The power of databases: the RRUFF project. In: Armbruster T, Danisi R (Eds.), Highlights in Mineralogical Crystallography. W. De Gruyter, Berlin, pp 1-30

Li J, Hitch M, Power I, Pan Y (2018) Integrated mineral carbonation of ultramafic mine deposits - A review. Minerals 8: 147. https://doi.org/10.3390/min8040147

Lomax G, Lenton TM, Adeosun A, Workman M (2015) Investing in negative emissions. Nat Clim Change 5: 498-500. https://doi.org/10.1038/nclimate2627

Meyer NA, Vogeli JU, Becker M, Broadhurst JL, Reid DL, Franzidis JP (2014.) Mineral carbonation of PGM mine tailings for CO_2 storage in South Africa: A case study. Min Eng 59: 45-51. https://doi.org/10.1016/j.mineng.2013.10.014

Mohamed S, van der Merwe EM, Altermann W, Doucet FJ (2016) Process development for elemental recovery from PGM tailings by thermochemical treatment: Preliminary major element extraction studies using ammonium sulphate as extracting agent. Waste Manage 50: 334-45. https://doi.org/10.1016/j.wasman.2016.02.021

Monasterio-Guillot L, Fernandez-Martinez A, Ruiz-Agudo E, Rodriguez-Navarro C (2021) Carbonation of calcium-magnesium pyroxenes: Physical-chemical controls and effects of reaction-driven fracturing. Geochim Cosmochim Acta 304: 258-280. https://doi.org/10.1016/j.gca.2021.02.016

Mondal SK, Mathez EA (2007) Origin of the UG2 chromitite layer, Bushveld Complex. J Petrol 48: 495-510. https://doi.org/10.1093/petrology/egl069

Morimoto N (1988) Nomenclature of pyroxenes. Mineral Petrol 39: 55-76.

Munz IA, Brandvoll O, Haug TA, Iden K, Smeets R, Kihle J, Johansen H (2012) Mechanisms and rates of plagioclase carbonation reactions. Geochim Cosmochim Acta 77: 27-51. https://doi.org/10.1016/j.gca.2011.10.036

Naraharisetti PK, Yeo TY, Bu J (2019) New classification of CO_2 mineralisation processes and economic evaluation. Renew Sustain Energy Rev, 99: 220-233. https://doi.org/10.1016/j.rser.2018.10.008

Northam Platinum Holdings Limited (2023) Operational and financial results for the year ended 30 June 2023. Northam, Rustenburg.

O'Connor WK, Dahlin DC, Nilsen DN, Rush GE, Walters RPTurner PC (2001) Carbon dioxide sequestration by direct mineral carbonation: results from recent studies and current status. Albany Research Center (ARC), Albany, OR.

O'Connor WK, Dahlin DC, Rush G, Gerdemann SJ, Penner L (2004) Energy and economic considerations for ex-situ and aqueous mineral carbonation, Albany Research Center (ARC), Albany, OR.

O'Connor WK, Dahlin DC, Rush G, Gerdemann SJ, Penner L (2005) Aqueous mineral carbonation. DOE/ARC-TR-04-002, Department of Energy, USA.

Oelkers EH, Schott J (1995) Experimental study of anorthite dissolution and the relative mechanism of feldspar hydrolysis. Geochim Cosmochim Acta 59(24): 5039-5053. https://doi.org/10.1016/0016-7037(95)00326-6

Oelkers EH, Schott J (2001) An experimental study of enstatite dissolution rates as a function of pH, temperature, and aqueous Mg and Si concentration, and the mechanism of pyroxene/pyroxenoid dissolution. Geochim Cosmochim Acta 65: 1219-1231. https://doi.org/10.1016/S0016-7037(00)00564-0

Olajire AA (2013) A review of mineral carbonation technology in sequestration of CO_2. J Pet Sci Eng 109: 364-392. https://doi.org/10.1016/j.petrol.2013.03.013

Peng D-Y, Robinson DB (1976) A new two-constant equation of state. Ind Eng Chem 15: 59-64.

Power IM, McCutcheon J, Harrison AL, Wilson S, Dipple GM, Kelly S, Southam C, Southam G (2014) Strategising carbon-neutral mines: A case for pilot projects. Minerals 4: 399-436. https://doi.org/10.3390/min4020399

Power I M, Paulo C, Rausis K (2024) The mining industry's role in enhanced weathering and mineralization for CO_2 removal. Environ Sci Tech 58: 43-53. https://doi.org/10.1021/acs.est.3c05081

Price JR, Velbel MA (2003) Chemical weathering indices applied to weathering profiles developed on heterogeneous felsic metamorphic parent rocks. Chem Geol 202: 397-416. https://doi.org/10.1016/j.chemgeo.2002.11.001

Prigiobbe V, Mazzotti M (2013) Precipitation of Mg-carbonates at elevated temperature and partial pressure of CO_2. Chem Eng J 223: 755-763. https://doi.org/10.1016/j.cej.2013.03.033

Sayles FL, Fyfe WS (1973) The crystallisation of magnesite from aqueous solution. Geochim Cosmochim Acta 37: 87-99. https://doi.org/10.1016/0016-7037(73)90246-9

Seifritz W (1990) CO_2 disposal by means of silicates. Nature 345: 486-486. https://doi.org/10.1038/345486b0

Sissmann O, Brunet F, Martinez I, Guyot F, Verlaguet A, Pinquier Y. & Daval D (2014) Enhanced olivine carbonation within a basalt as compared to single-phase experiments: Reevaluating the potential of CO_2 mineral sequestration. Environ Sci Tech, 48: 5512-5519. https://doi.org/10.1021/es405508a

Stokreef S, Sadri F, Stokreef A, Ghahreman A (2022) Mineral carbonation of ultramafic tailings: A review of reaction mechanisms and kinetics, industry case studies, and modelling. CLCE 8: 100491

Tibane L, Pöllmann H, Ndongani F, Landman B, Altermann W (2021) Evaluation of the lithofacies, petrography, mineralogy, and geochemistry of the onshore Cretaceous Zululand Basin in South Africa for geological CO_2 storage. Int J Greenhouse Gas Control 109: 103364. https://doi.org/10.1016/j.ijggc.2021.103364

Veetil SKP, Hitch M (2021) Aqueous mineral carbonation of ultramafic material: a pre-requisite to integrate into mineral extraction and tailings management operation. Environ Sci Pollut Res 28, 29096–29109. http://doi.org/ 10.1007/s11356-021-12481-0

Vogeli J, Reid DL, Becker M, Broadhurst J, Franzidis JP (2011) Investigation of the potential for mineral carbonation of PGM tailings in South Africa. Miner Eng 24: 1348-1356. https://doi.org/10.1016/j.mineng.2011.07.005

Wilson MJ (2004) Weathering of the primary rock-forming minerals: processes, products and rates. Clay Miner. 39: 233-266. http://doi.org/10.1180/0009855043930133

WMO (2023) The State of Greenhouse Gases in the Atmosphere Based on Global Observations through 2022. WMO Greenhouse Gas Bulletin. Geneva: World Meteorological Organization.

Yadav S, Mehra A (2022) A review on ex situ mineral carbonation. Environ Sci Pollut Res 28: 12202-12231. https://doi.org/ 10.1007/s11356-020-12049-4

Zeh A, Ovtcharova M, Wilson, A H & Schaltegger U (2015) The Bushveld Complex was emplaced and cooled in less than one million years – results of zirconology, and geotectonic implications. Earth Planet Sci Lett 418: 103-114. https://doi.org/ 10.1016/j.epsl.2015.02.035

Zimmerman GH, Staros DJ, Arcis H (2022) Critical Review of Transport and Equilibrium Properties of Potassium Chloride in High Temperature Water. J. Chem. Eng. Data 67: 533-544. https://doi.org/10.1021/acs.jced.1c00814

Statements and Declarations

Ethical approval

Not applicable

Consent to participate

All the authors (Zakhele H. Nkosia, Wladyslaw Altermann, Herbert Pölmann, Frédéric J. Doucet) consented to participate in this research.

Consent to publish

All the authors (Zakhele H. Nkosia, Wladyslaw Altermann, Herbert Pölmann, Frédéric J. Doucet) consented to publish and co-author this research.

Author contributions

Zakhele H. Nkosia, Wladyslaw Altermann, Herbert Pölmann and Frédéric J. Doucet contributed to the study conception and design. Material preparation, data collection and analysis were performed by Zakhele H. Nkosi. The first draft of the manuscript was written by Zakhele Nkosi, and Wladyslaw Altermann and Frédéric J. Doucet commented on previous versions of the manuscript. Zakhele H. Nkosia, Wladyslaw Altermann and Frédéric J. Doucet read and approved the final manuscript. Herbert Pölmann passed away before the submission of the manuscript.

Funding

This work was supported by CIMERA (DST-NRF Centre of Excellence for Integrated Mineral and Energy Resources Analysis; Grant 91487) and the National Research Foundation (Grant 88119) through the DAAD-NRF scholarship programme.

Competing interests

The authors have no relevant financial or non-financial interests to disclose.

Data availability statement

Data generated during the study is provided within the manuscript or supplementary information files. Raw data is available from the corresponding author on request.